Effects of Meteorological and Hydrological Changes on Ground-Strain Measurements

AUTHOR(S):

TAKEMOTO, Shuzo

CITATION:

TAKEMOTO, Shuzo. Effects of Meteorological and Hydrological Changes on Ground-Strain Measurements. Bulletin of the Disaster Prevention Research Institute 1983, 33(1): 15-46

ISSUE DATE:

1983-03

URL:

http://hdl.handle.net/2433/124915

Effects of Meteorological and Hydrological Changes on Ground-Strain Measurements

By Shuzo TAKEMOTO

(Manuscript received December 11, 1982)

Abstract

Using continuous records obtained from four extensometers with laser interferometer systems at the Amagase Observatory, effects of meteorological and hydrological changes on ground-strain measurements have been investigated.

Seasonal variations with a strain amplitude of the order of 10^{-6} have been observed with horizontal and vertical componetns in directions normal to the axis of the observation tunnel over a period of thirteen months. On the other hand, seasonal variations observed with horizontal components along the tunnel are smaller than 1×10^{-7}. As a possible source of these variations, we consider the hydrological perturbation due to the seasonal variation of the groundwater pressure around the observation tunnel.

After removing seasonal variations from observed data of ground-strains, there remain transient variations of the order of 10^{-7} in components normal to the tunnel. While, variations of this sort are not found in components along the tunnel. These transient variations cannot be explained by the elastic strains caused by the negative surface-load due to the passage of the typhoon or due to the fluctuation of the water level in a nearby reservoir, but can be explained by the hydrological effect of groundwater pressures in pores of a porous medium under the rapid draw-up or draw-down of the water level of the reservoir.

1. Introduction

For the purpose of precise measurements of ground-strains, we have developed some types of extensometers with laser interferometer systems (Takemoto[1], hereafter referred to as Paper I, and Takemoto and Kobayashi[2]). These instruments were installed in the tunnel at the Amagase Crustal Movement Observatory and quantitative measurements of ground-strains in terms of the wavelength of He-Ne laser light have been carried on since 1978.

Using continuous records obtained from these instruments for a period of 390 days, we have calculated the amplitudes and phase lags of tidal strains by the least squares method. By comparing these values with theoretically expected tidal strains, we have evaluated the effects of local inhomogeneities on ground-strain measurements (Takemoto[3], hereafter referred to as Paper II). The results of Paper II are as follows: (1) Amplitude enhancements of tidal strains observed with the horizontal and vertical extensometers normal to the axis of the tunnel are well explained by the cavity effect calculated by the two-dimensional finite element techniques for the actual cross-section of the horseshoe shaped tunnel. In this case, the apparent strain observed with the horizontal component across the tunnel is about 2.4 times larger

than the applied strain in the same direction in the absence of the tunnel. (2) The distortion of the strain field due to the topographic effect, which was calculated by the three-dimensional finite element techniques, is smaller than 10% of the applied strain field in this region.

To derive useful information of regional strain fields associated with tide generating forces or tectonic origins, there exist some fundamental problems of ground-strain measurements carried on near the earth's surface. The first of these is the reliability of instruments and adequacy of their coupling with base rocks. The second is the distortion of the applied strain field due to local inhomogeneities around the observation site. The third is the existence of noise generated at the earth's surface by non-tectonic origins, i.e. meteorological and hydrological perturbations. The first and second problems were previously discussed in Paper I and Paper II, respectively. We now discuss the third problem in this paper.

Effects of meteorological changes on ground-strain measurements have been discussed by many workers in many observatories. The effects especially due to the rainfall and air temperature change are dominant at some observatories, such as Ide (Takada[4]), Iwakura (Takemoto[5], and Takada et al.[6]), Oura and Akibasan (Tanaka[7]). A common feature for these observatories is that all instruments were installed at shallow depths (<30 m). On the contrary, instruments of the Amagase Observatory are installed at positions of 400$\sim$500 m from the entrance of the tunnel having a length of 1830 m. The depth of the observation site from the earth's surface is about 140 m. For such a deep tunnel, meteorological perturbations are considerd to be small compared with those for other shallow observatories. Taking this aspect into consideration, we investigate the seasonal variations of ground-strains observed with four extensometers with laser interferometer systems. We further investigate the effect of barometric change on ground-strain measurements for the case of passage of a typhoon near the observation site. Assuming that the change of the atmospheric pressure caused by the passage of a typhoon is a negative load acting on a homogeneous and isotropic semi-infinite elastic body, we estimate the elastic strain field expected at the observation site and thereafter we compare it with the observed ground-strains.

In respect to the hydrological effect on ground-strain measurements peculiar to the Amagase Observatory, transient variations of the order of 10^{-7} in a strain amplitude have been often observed in horizontal and vertical components normal to the tunnel at the time of rapid draw-up or draw-down of the water level of the reservoir located at several hundred meters from the observation site (Takemoto[8]). In order to obtain physical interpretation of this mechanism, we investigate the stress-strain relations of impermeable and permeable models under the rapid draw-down of the water level of the reservoir using the two-dimensional finite element techniques. In the latter case, the seepage of groundwater in a porous medium around the tunnel is taken into consideration and the effect of groundwater pressure on strains in a porous medium is analyzed in detail.

2. Instrumentation

The Amagase Observatory is located in the southern part of Kyoto Prefecture. The topographic map around the observation site and its cross-section in the direction toward the Amagase dam are shown in **Fig. 1**. In the disused race tunnel of the hydraulic power station, super-invar bar extensometers, a super-invar wire extensometer, tiltmeters of horizontal pendulum type and water-tube tiltmeters were installed and continuous observations of ground-strains and -tilts have been carried on since 1967 (Takada et al.[9]).

In addition to these instruments, four extensometers with laser interferometer systems were installed in 1977~1978. Two of them (EL–1 and EL–V) are super-invar bar extensometers with laser interferometer systems consisting of simple laser sources, Michelson interferometers and photo-detecting equipments with image sensors. The remaining two components (L–1 and L–2) are laser extensometers with a frequency-stabilized laser source and evacuated light paths. The designs of these instruments are given in Paper I.

EL–1 and L–1 components are orientated along the tunnel and the L–2 component is across the tunnel. The EL–V is a vertical component installed between the ceiling and the concrete base fixed on the rock under the floor of the tunnel. Resolving powers and other numerical constants of these instruments are given in **Table 1.**

Table 1. Constants of laser extensometers at the Amagase Observatory (34°53′N, 135°50′E).

Mark	Azimuth	Span	Resolving Power
L–1	N72.5°W	15.8 m	1.0×10^{-9} strain
L–2	N17.5°E	3.2 "	5.0 "
EL–1	N72.5°W	40.0 "	0.25 "
EL–V	Vertical	6.4 "*	1.5 "

* total length containing standard bar and concrete base.

3. Observational Results

3.1. Seasonal Variations of Ground-Strains

Seasonal variations of ground-strains have been derived by eliminating linear trends and tidal strains from the hourly data of the four extensometers for the period from March 07 1979 to March 31 1980. Eliminations of tidal strains are carried out with the Pertzev's filter.

Results are shown in **Fig. 2(A)**, together with the amount of precipitation. **Fig. 2(B)** shows variations of the water level and water discharge of the Amagase Reservoir. These hydrological data were supplied from the Amagase Dam Control Office of the Kinki Regional Construction Bureau, Ministry of Construction.

As shown in **Fig. 2(A)**, remarkable variations with a strain amplitude of the

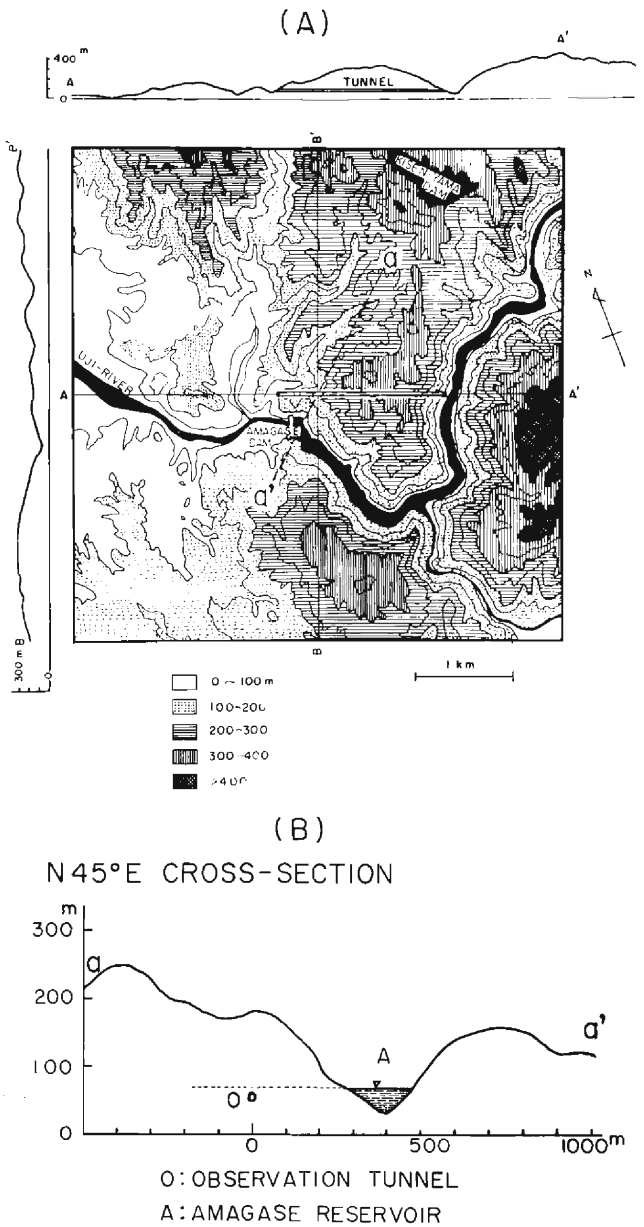

Fig. 1. Topographic map around the Amagase Observatory (upper), and its cross-section in the direction toward the Amagase dam (a-a′ section) (lower).

order of 10^{-6} are found in the horizontal and vertical components normal to the tunnel (L–2 and EL–V). On the other hand, seasonal variations of the horizontal components along the tunnel (L–1 and EL–1) are smaller than 1×10^{-7} over the period of thirteen months. As a general tendency, seasonal variations of ground-strains do not show a sinusoidal curve as was expected from the thermal effect due to the seasonal variation of air temperature. This tendency is consistent with other observational results obtained from other extensometers and tiltmeters at the same tunnel for the period from 1967 to 1981 (Takada et al.[9]). We thus consider that the thermal effect on long term variations of ground-strains are not so dominant at the Amagase Observatory.

If examined in detail, the variations of L–2 and EL–V components show contraction of 1.8×10^{-6} and extension of 1.1×10^{-6}, respectively, for the period from April to May of 1979. The trends reversed in June 1979 and again reversed in the first half of July 1979. Then, these strains gradually recovered. Comparing these variations with the precipitation, the effect of rainfall on ground-strains are also not so distinct except for the period of the first half of July 1979, when it went on raining from June 27 to July 07 of 1979, and the total amount of precipitation through eleven days came to 216 mm. Because of this heavy rainfall, the L–2 component contracted to the amount of 0.9×10^{-6} and the EL–V component extended to the amount of 0.5×10^{-6}. However, more distinct variations before this heavy rainfall are not correlative to the amount of precipitation.

We next compare these variations of ground-strain with the hydrological data of the Amagase Reservoir. As shown in **Fig. 2(B)**, the water level of the reservoir is controlled so as to be at a high level of about 75 m in dry seasons and to be at a lower level of about 68 m in rainy seasons. The amount of discharge is ordinarily less than 100 m^3/sec but it exceeded 400 m^3/sec during May and July of 1979. Comparing these factors with seasonal variations of ground-strains, we can find no distinct correlation between them.

As a result, seasonal variations of ground-strains at this observatory are not directly affected by individual perturbation factors such as the rainfall, variations of the water level and water discharge of the nearby reservoir, but are affected by the 'synthetic' hydrological perturbation factor in which the groundwater seepage around the tunnel plays an important role. We will discuss this later in section 7.

3.2. Transient Variations of Ground-Strains

In addition to seasonal variations of the order of 10^{-6}, transient variations of the order of 10^{-7} are found in L–2 and EL–V components of **Fig. 2(A)** at the end of September 1979, the middle of October 1979, the end of December 1979 and the end of February 1980. These variations are closely related to transient variations of the water level of the reservoir shown in **Fig. 2(B)**.

The relationship between ground-strains and the water level of the reservoir are investigated in detail for the period from September 18 to October 31, 1979.

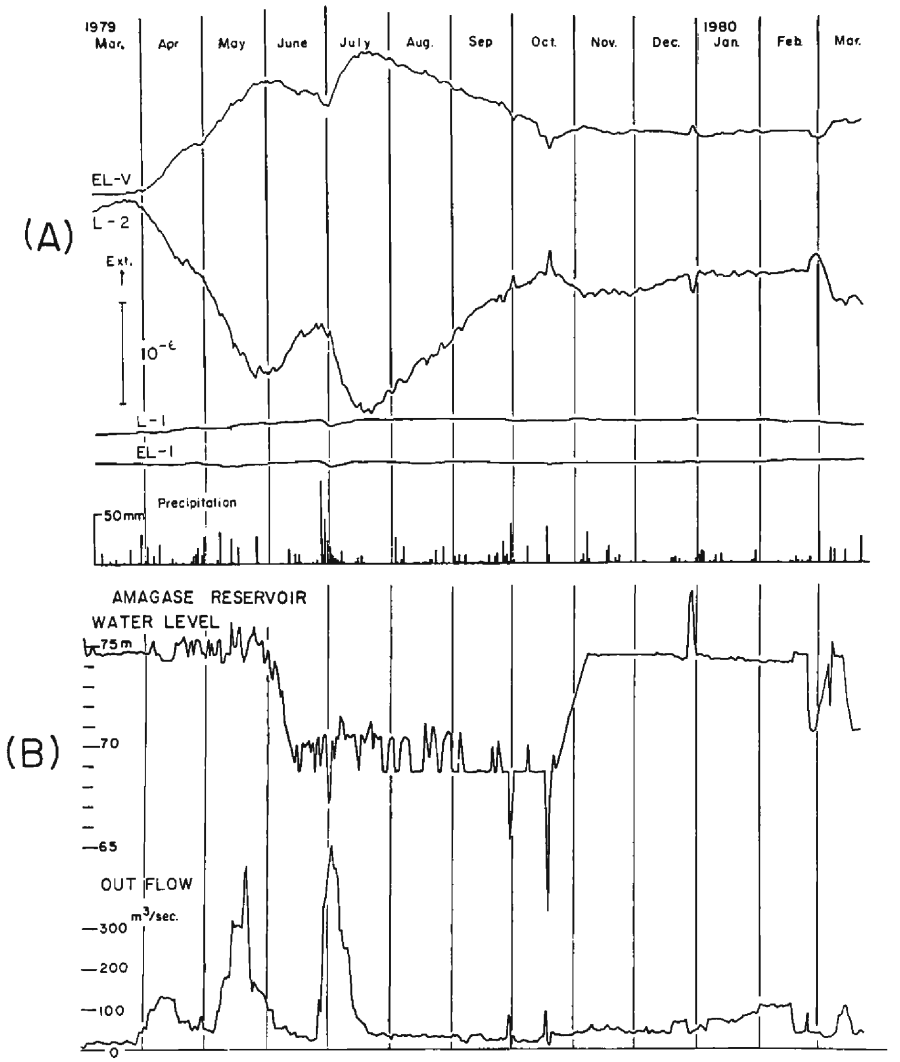

Fig. 2. Seasonal variations of ground-strains and precipitation (upper), and variations of water level and water discharge of the Amagase Reservoir (lower).

Fig. 3(**A**) shows hourly data of ground-strains for the period of 40 days, together with barometric data and precipitation. **Fig. 3**(**B**) shows the equally-weighted running means of twentyfive consecutive data of ground-strains and **Fig. 3**(**C**) shows the daily mean water levels of the reservoir.

Comparing (**B**) and (**C**) of **Fig. 3,** there exist distinct correlations between them. As shown in **Fig. 3** with marks of (**a**), (**b**) and (**d**), the L–2 component contracted and the EL–V component extended because of the rapid draw-up of the water level of the reservoir. On the contrary, because of the rapid draw-down of the water

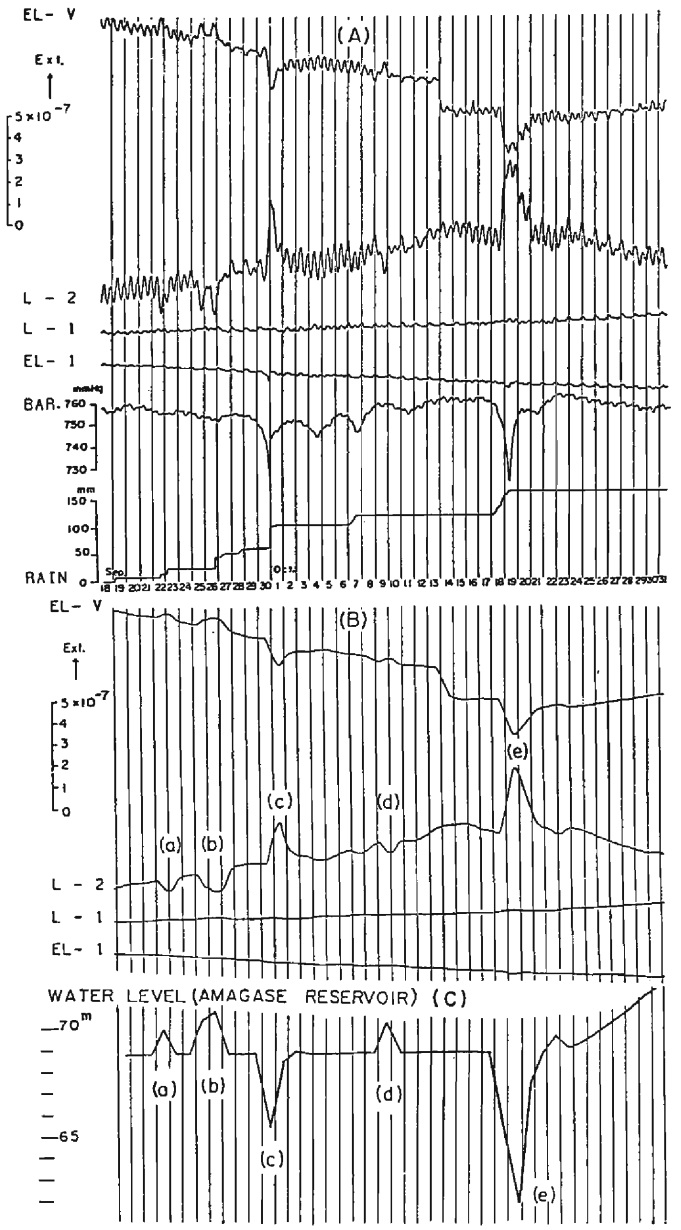

Fig. 3. (A): Hourly records of ground-strains, together with barogram and precipitation for the period from September 18 to October 31, 1979.
(B): 25 hours running means of ground-strains.
(C): Daily mean of water level of the Amagase Reservoir.

level as shown in this figure labelled (**c**) and (**e**), the L–2 component extended and the EL–V component contracted. In all cases of (**a**)~(**e**), the amplitude ratio of variations of L–2 and EL–V components is about 2:1. On the other hand, L–1 and EL–1 components are not so much affected by the variations of the water level of the reservoir.

Fig. 4 shows the schematic diagram of ground-strains around the tunnel associated with the rapid draw-up of the water level of the reservoir, where the direction x is along the tunnel, y across the tunnel and z the vertical. Because of the draw-up of 10 m of the water level, the y component contracts and the z component extends with a strain amplitude of the order of 10^{-7}. The x component is not affected at that time.

For the occasions of (**c**) and (**e**) in **Fig. 3,** two typhoons (T7916 and T7920) passed through the southern part of Kinki district and accordingly remarkable baro-

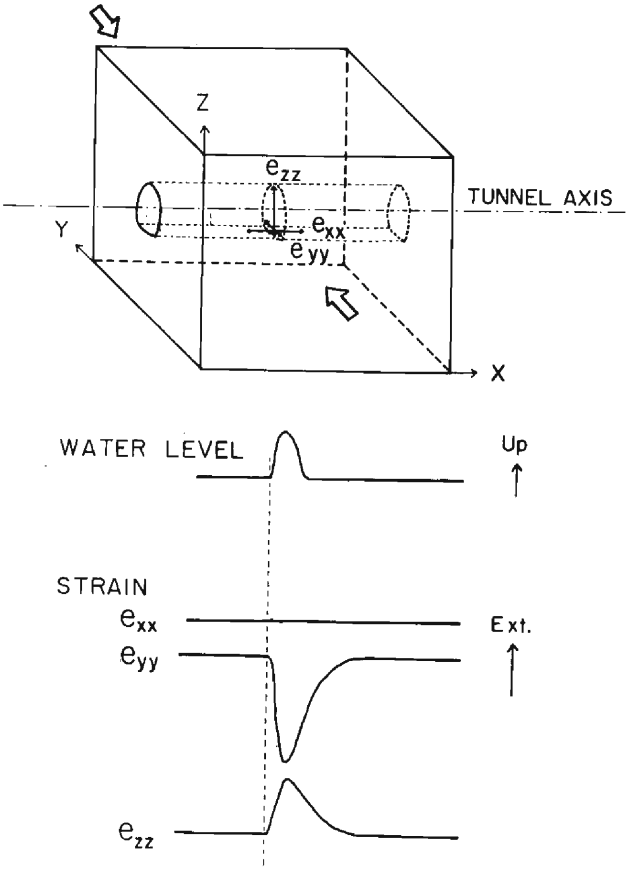

Fig. 4. Schematic diagram showing strain distributions around the observation tunnel caused by the rapid draw-up of water level of the reservoir.

metric changes are found in **Fig. 3**(**A**). Therefore, it is necessary to investigate whether these ground-strains are caused by the atmospheric loading effect due to the passage of typhoons or caused by the hydrological effect under the rapid draw-down of the water level of the reservoir. We begin with the analysis of elastic strains associated with the passage of typhoons.

4. Analysis of Elastic Strains Associated with the Passage of Typhoons

Assuming that the change of the atmospheric pressure due to the passage of a typhoon is a negative load acting on a homogeneous and isotropic semi-infinite elastic body, we have analyzed elastic strains around the tunnel near the earth's surface.

Paths of the two typhoons are shown in **Fig. 5.** Numerical calculations of elastic strains are only made for the case of T7916 which landed at Osaka at 23 h on September 30 1979 and passed through the neighborhood of the Amagase Observatory. Local weather maps for the period from 20 h on September 30 to 01 h on October 01 are shown in **Fig. 6** (referred to Nakajima et al.[11]).

For estimating analytical solutions, we adopt the theoretical expressions of pressure and displacement fields given by Trubitsyn and Makalkin[12]. According to their expressions, the surface load due to the symmetric distribution of atmospheric pressure is approximated by the following equation in the cylindrical coordinate system (r, θ, z),

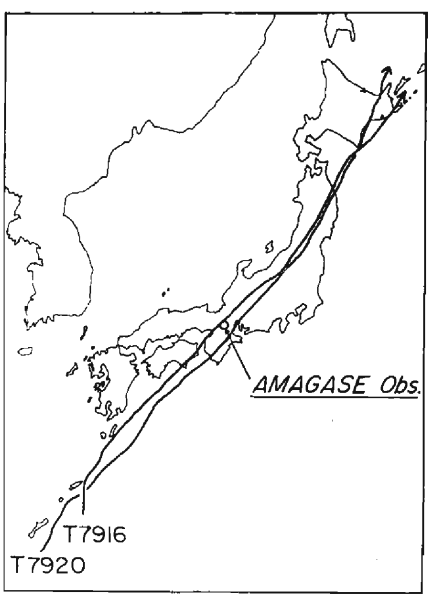

Fig. 5. Paths of two typhoons which passed through the southern part of Kinki district in 1979.

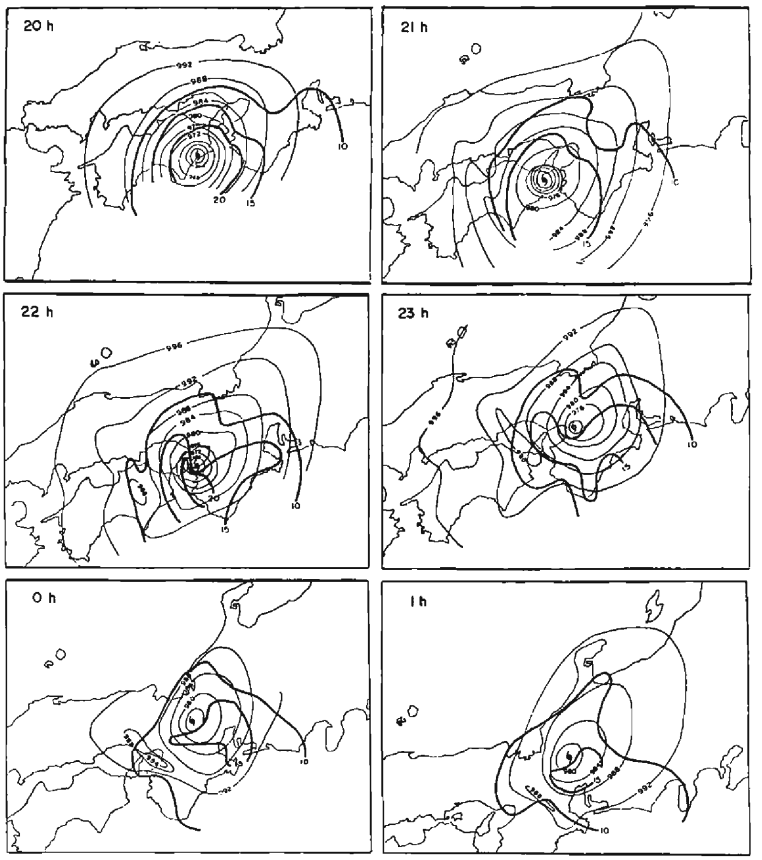

Fig. 6. Local weather maps from 20 h on September 30 to 01 h on October 01. Isobaric lines shown by thin curves are in mb, contours of the wind speed shown by thick curves are in m/sec (After Nakajima et al.[11]).

$$P(r) = P_0(1+r^2/r_0^2)^{-3/2}, \tag{1}$$

where P_0 and r_0 are constants defining the intensity and volume of a typhoon.

Displacements of a semi-infinite elastic body bounded by the infinite plane $z=0$ under the normal load P are given as follows,

$$\left.\begin{aligned} u_r &= \frac{1}{2\mu}P_0 r_0^2\left[-(1-2\nu)\frac{r}{r_0+z+D}+\frac{zr}{D}\right]\frac{1}{D} \\ u_\theta &= 0 \\ u_z &= \frac{1}{2\mu}P_0 r_0^2\left[2(1-\nu)+\frac{z(r_0+z)}{D^2}\right]\frac{1}{D} \end{aligned}\right\} \tag{2}$$

where $D^2=(r_0+z)^2+r^2$, and μ and ν are the rigidity and Poisson's ratio, respectively.

Displacements, linear strains and tilt at $z=0$ are derived from Eqs. (2) as follows,

$$\left.\begin{aligned} u_r &= \frac{1}{2\mu} P_0 r_0^2 \left[-(1-2\nu)\frac{r}{r_0+d} \right] \frac{1}{d} \\ u_\theta &= 0 \\ u_z &= \frac{1}{\mu} P_0 r_0^2 (1-\nu) \frac{1}{d} \end{aligned}\right\} \tag{3}$$

$$\left.\begin{aligned} \varepsilon_r &= \frac{\partial u_r}{\partial r} = -\frac{1}{2\mu} P_0 r_0^2 (1-2\nu) \left[\frac{1}{(r_0+d)d} - \frac{r^2}{(r_0+d)d^3} - \frac{r^2}{(r_0+d)^2 d^2} \right] \\ \varepsilon_\theta &= \frac{u_r}{r} + \frac{\partial u_\theta}{r\partial\theta} = -\frac{1}{2\mu} P_0 r_0^2 (1-2\nu) \left[\frac{1}{(r_0+d)d} \right] \\ \varepsilon_z &= \frac{\partial u_z}{\partial z} = -\frac{1}{2\mu} P_0 r_0^3 (1-2\nu) \left[\frac{1}{d^3} \right] \\ \tau_r &= \frac{\partial u_z}{\partial r} = -\frac{1}{\mu} P_0 r_0^2 (1-\nu) \left[\frac{r}{d^3} \right] \end{aligned}\right\} \tag{4}$$

where $d^2=r_0^2+r^2$.

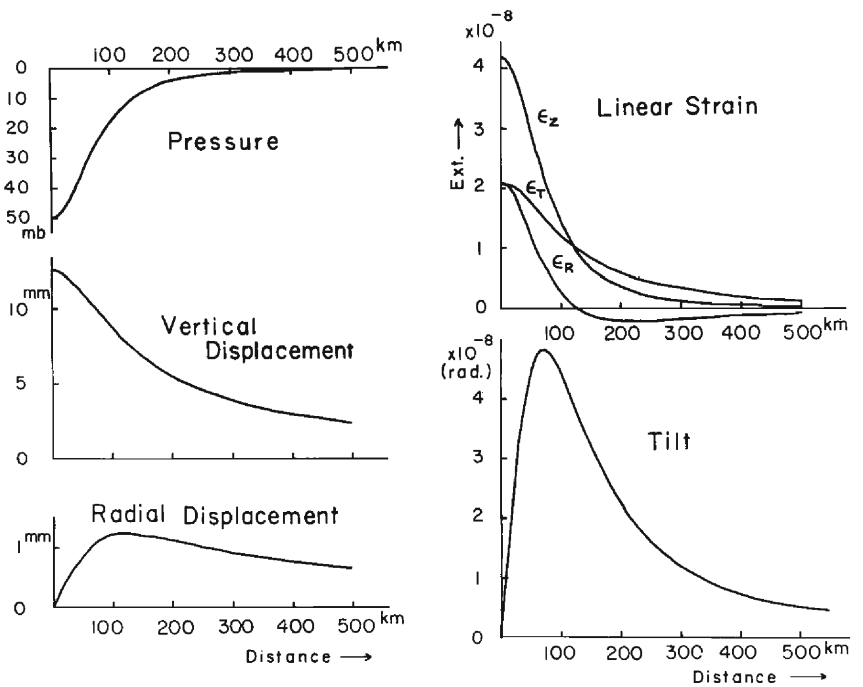

Fig. 7. Pressure distribution obtained by substituting $r_0=100$ km and $p_0=-50$ mb into equation (1), and displacement, strain and tilt fields induced by the surface pressure.

As an example of numerical calculations, **Fig. 7** shows displacements, linear strains and tilt obtained for the free surface by setting $P_0=-50$ mb, $r_0=100$ km, $\mu=3\times10^{10}$ N/m^2 and $\nu=0.25$. As shown in this figure, linear strains attain the maximum extensions of 4.2×10^{-8} (ε_z) and of 2.1×10^{-8} (ε_r and ε_θ) at the center of the typhoon and these values are gradually decreasing in amount of extension toward the perimeter. Ultimately at the far field ($r>4r_0$), $\varepsilon_z\fallingdotseq0$ and $\varepsilon_r\fallingdotseq-\varepsilon_\theta$.

Using the same model, we estimated the strain field due to the passage of T7916. In **Fig. 8**, the solid curves show the pressure profiles in the North-South and East-West directions at 23 h on September 30, and the broken curves show the approximated ones with Eq. 1 by setting $P_0=-30$ mb and $r_0=100$ km. These curves fairly well fit each other. Then, we estimated the strain field under the assumption that a hypothetical typhoon with a pressure profile given by the broken curve of **Fig. 8** passed along the path shown in **Fig. 5.** In this procedure, the existence of water mass in seas is disregarded and calculations are made for the semi-infinite elastic body having values of $\mu=1.73\times10^{10}$ N/m^2 and $\nu=0.279$.

As a result, the maximum strain changes due to the passage of T7916 are expected at the Amagase Observatory as follows:

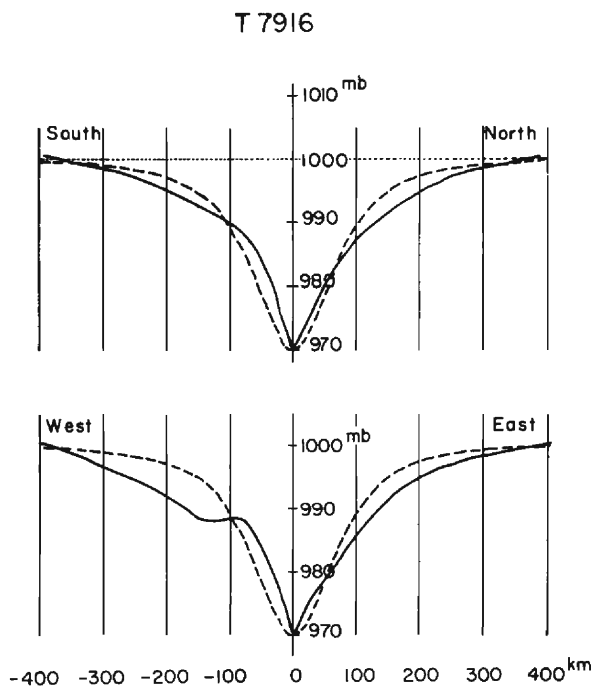

Fig. 8. Pressure profiles in North-South and East-West directions at 23 h on September 30 (solid curve) and approximated curve using equation (1) (broken curve).

$$\varepsilon_r = 1.9\times10^{-8}$$
$$\varepsilon_\theta = 1.9\times10^{-8}$$
$$\varepsilon_z = 3.8\times10^{-8}\,.$$

These values have been determined under free surface conditions but the practical observation of ground-strain was carried on in the tunnel near the surface. Therefore it is necessary to consider the cavity effect on strains. We investigated this effect using the finite element techniques. Hereafter, we will adopt the rectangular coordinate system with directions x along the tunnel, y across the tunnel and z vertical.

Assuming that the center of the typhoon is located just above the observation site, the normal stress components near the surface of the semi-infinite elastic body can be expressed as follows:

$$\left.\begin{aligned}\sigma_x^0 &= \sigma_y^0 = -(1+2\nu)/2\times P_0\\ \sigma_z^0 &= -P_0\,.\end{aligned}\right\} \qquad (5)$$

and the linear strain components are similarly,

$$\left.\begin{aligned}e_{xx}^0 &= e_{yy}^0 = -(1-2\nu)/4\mu\times P_0\\ e_{zz}^0 &= -(1-2\nu)/2\mu\times P_0\,.\end{aligned}\right\} \qquad (6)$$

and shearing components of stress and strain do not exist in this problem. We use the notation $(e_{xx}^0,\ e_{yy}^0,\ e_{zz}^0)$ for linear strains which should be observed in the absence of the cavity and $(e_{xx}^c,\ e_{yy}^c,\ e_{zz}^c)$ for those around the cavity.

It is reasonable to consider that the linear strain in the direction along the tunnel is not affected by the cavity effect (Panek[13]). We now investigate the distortion of linear strains in y and z components due to the cavity effect. For the present purpose, we use a two-dimensional finite element model which is shown on the left hand of **Fig. 9.** As boundary conditions, nodal forces equivalent to $\sigma_y^0=-(1+2\nu)/2\times P_0$ are applied on faces AD and BC and similarly nodal forces equivalent to $\sigma_z^0=-P_0$ are applied on faces AB and DC. In addition to these, nodal forces equivalent to the hydrostatic pressure $(-P_0)$ are applied on the wall around the cavity. Assuming the mirror image symmetry, calculations are made only for the half-plate EFCB, which is divided into 161 triangular elements with 104 nodes. Along the line EF, nodal displacements of the y direction are fixed to be zero.

Putting $P_0=-30$ mb, $\mu=1.73\times10^{10}$ N/m^2 and $\nu=0.279$, nodal displacements around the cavity are calculated under the plane strain condition. Consequently, 'apparent strains' around the cavity ($e_{yy}^{c'}$ and $e_{zz}^{c'}$) are calculated. The total strain field around the cavity is determined by adding contributions from the linear strain component along the tunnel (e_{xx}^0) to $e_{yy}^{c'}$ and $e_{zz}^{c'}$ which are calculated under the plane strain condition with respect to the $y-z$ plane. Then,

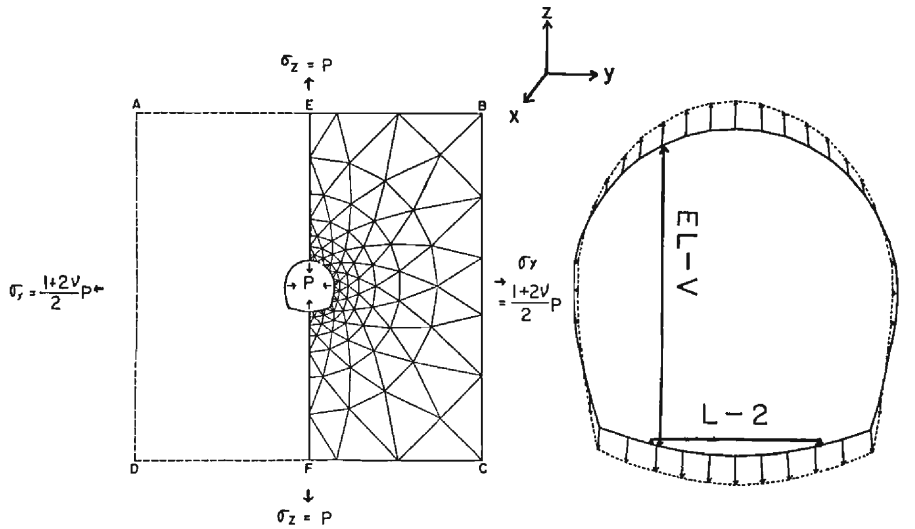

Fig. 9. Finite element model used for calculations of cavity effects (left) and deformation of cavity caused by the passage of typhoon (right), where $P=-P_0$.

$$\left.\begin{aligned} e^c_{xx} &= e^0_{xx} \\ e^c_{yy} &= e^{c'}_{yy} - \nu e^0_{xx} \\ e^c_{zz} &= e^{c'}_{zz} - \nu e^0_{xx} . \end{aligned}\right\} \qquad (7)$$

Finally, values of e^c_{xx}, e^c_{yy} and e^c_{zz} at the place where instruments are installed are obtained as follows:

$$\begin{aligned} e^c_{xx} &= 1.9\times10^{-8} \\ e^c_{yy} &= 0.4\times10^{-8} \\ e^c_{zz} &= 5.1\times10^{-8} . \end{aligned}$$

Deformation of the cross-section of the tunnel is shown on the right hand of **Fig. 9.**

On the other hand, observed strains during the interval from 19 h on September 30 to 02 h on October 01 were obtained as follows:

$$\begin{aligned} (e_{xx})_{\text{obs}} &= \quad 0.0(-1.0\times10^{-8} < (e_{xx})_{\text{obs}} < 1.0\times10^{-8}) \\ (e_{yy})_{\text{obs}} &= \quad 3.6\times10^{-7} \\ (e_{zz})_{\text{obs}} &= -1.8\times10^{-7} , \end{aligned}$$

where the negative sign indicates the contraction. Components of tidal strains were previously subtracted from original data.

Comparing these values with the theoretically expected ones for the atmospheric loading effect due to the passage of the typhoon, there is poor correlation between them. In the x direction, the ground-strain exceeding 1×10^{-8} was not observed. The observed value in y direction is more than one order larger than the expected one. In an extreme case, observed and expected values have the opposite sign in the

z direction.

As a result, we consider that variations of ground-strains shown in **Fig. 3** with marks of (**c**) and (**e**) were not caused by the passage of the typhoon but were caused by the rapid draw-down of the water level of the reservoir. Therefore, we will investigate stress-strain relations in a porous medium under the rapid draw-down of the water level of the reservoir. In these treatments, we will use the two-dimensional finite element models with respect to the $y-z$ plane, because the variation of ground-strain in x direction is negligibly small and the plane strain condition is acceptable.

5. Analysis of Stress-Strain Relations in the Porous Medium under the Rapid Draw-down of the Water Level of the Reservoir

5.1. Impermeable Elastic Model

Generally, rocks near the earth's surface may be considered to be a porous and

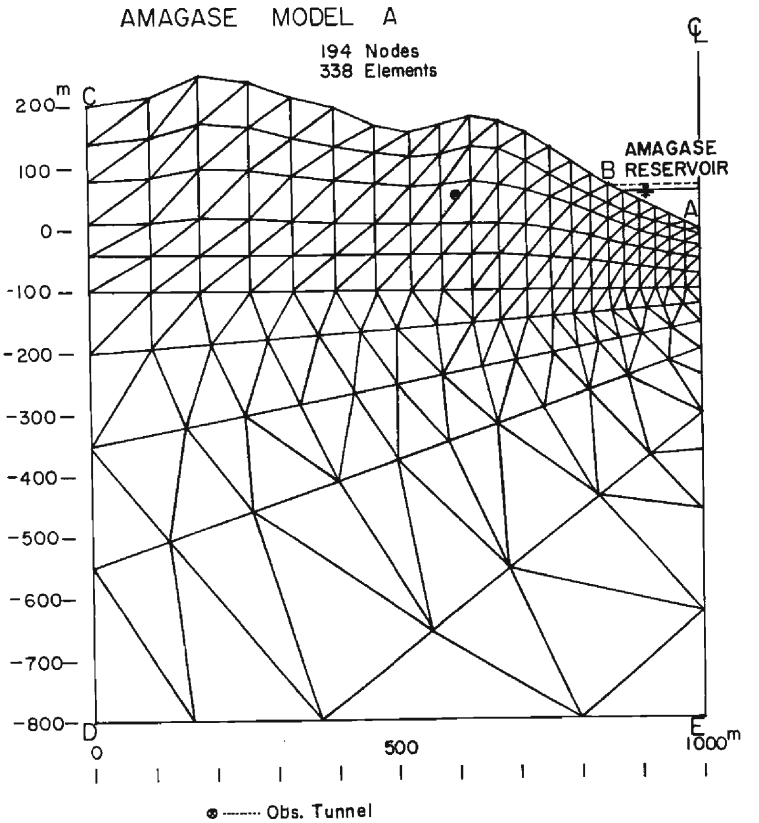

Fig. 10. Finite element model expressing the region of about 1000×1000 m with 338 triangular elements.

permeable medium. However the medium is firstly assumed to be an impermeable elastic body where the seepage of water through the medium does not enter into the problem and the rapid draw-down of the water level of the reservoir is simply treated as a negative load acting on the surface of the homogeneous and isotropic elastic body. The analysis of stress-strain relations has been made by the two-dimensional finite element method.

As shown in **Fig. 10,** the region of about 1000 m × 1000 m including the observation tunnel (⊗) is expressed as an assembly of 338 triangular elements with 194

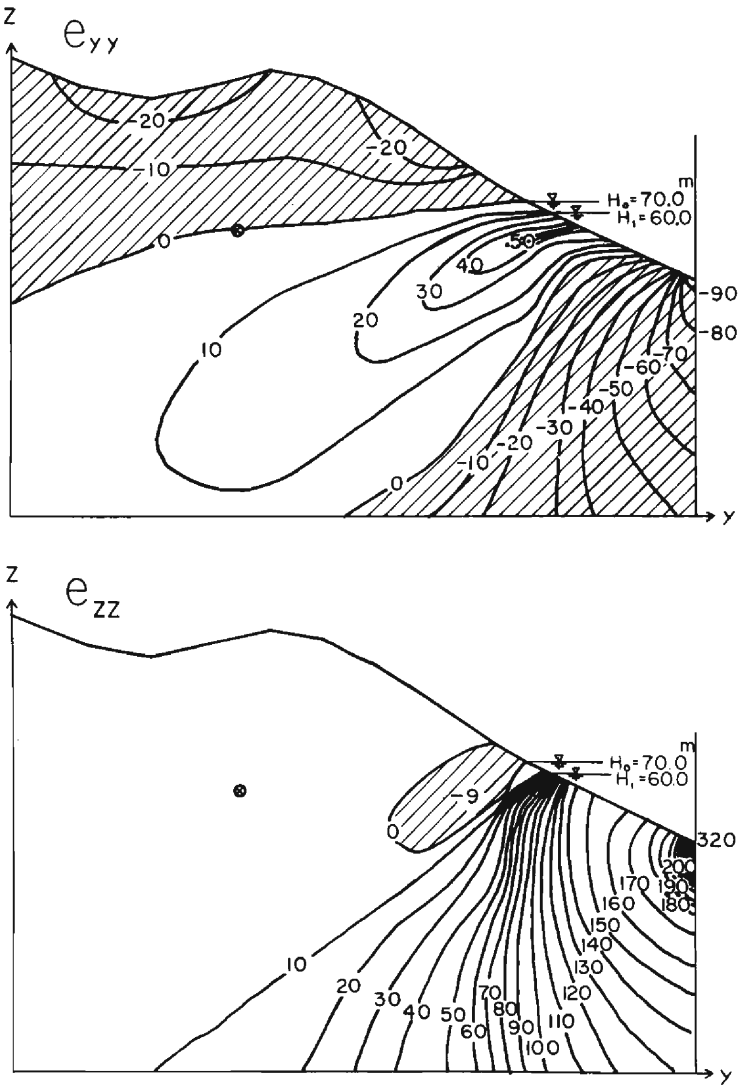

Fig. 11. Distributions of strains associated with the negative surface-load under the rapid draw-down of the reservoir ($\times 10^{-8}$).

nodes. As boundary conditions, horizontal displacements on faces AE and DE, and vertical displacements on the face DE are fixed to be zero. The negative load acting on the surface AB is given by the rapid draw-down of the water level of the reservoir from an elevation of 70 m to an elevation of 60 m. The values of Young's modulus (E) and Poisson's ratio (ν) are set to be $4.49\times10^{10}\mathrm{N/m^2}$ and 0.279, respectively. These values are assumed to be the same for all elements.

Linear strains in the horizontal and vertical directions (e_{yy}, e_{zz}) have been calculated under the plane strain condition and contour plots of these strains are shown in **Fig. 11.** At the position of the tunnel ($\otimes$), both components of e_{yy} and e_{zz} are in order of 10^{-8} and these values are an order of magnitude smaller than the observed ones.

This result shows that the variations of ground-strains observed at the Amagase Observatory under the rapid draw-down of the water level of the reservoir cannot be explained by the impermeable elastic model. Therefore we consider in the following subsection the effect of groundwater pressure on strains in a porous and permeable medium.

5.2. Porous and Permeable Model

5.2.1. Steady and Unsteady Seepage through the Porous Medium

For the present purpose, the flow through the pores in a porous medium is assumed to be based on Darcy's Law which establishes a linear relationship between the seepage velocity ($\boldsymbol{V}_D$) and the gradient of hydraulic head ($\boldsymbol{H}$) as follows;

$$\{\boldsymbol{V}_D\} = -\boldsymbol{K}\{\mathrm{grad}\,\boldsymbol{H}\}\,, \tag{8}$$

where $\boldsymbol{K}$ is the coefficient of permeability. The negative sign indicates that the velocity is in a direction of decreasing the hydraulic head.

For the flow of steady seepage, the equation of continuity is,

$$\mathrm{div}\,\{\boldsymbol{V}_D\} = 0\,. \tag{9}$$

Substituting Eq. 8 into Eq. 9, we obtain the governing differential equation as follows;

$$\mathrm{div}\,\{\boldsymbol{K}\,\mathrm{grad}\,\boldsymbol{H}\} = 0\,. \tag{10}$$

Eq. 10 has an infinite number of solutions and a unique solution can only be obtained when the boundary conditions of the flow domain are fully specified.

For the solution of boundary value problems governed by Eq. 10, Zienkiewicz et al.[14] first introduced a finite element approach with a network of linear triangular elements. Using a similar network, Taylor and Brown[15], Finn[16] and Kawamoto et al.[17] extended this method to include problems of steady seepage with a free surface. In their procedures, the free surface was initially guessed and subsequently adjusted by iterative procedures until the free boundary conditions were satisfied. Unsteady

seepage problems where the free surface was continuously changing with time were solved by France et al.[18] and Desai[19] by considering the solution to be a series of steady state solutions at small intervals of time Δt apart.

Referring to these procedures, we analyze the problem of seepage through the porous medium on an impermeable foundation shown in **Fig. 12.** Herein we assume that the groundwater in the medium is supplied from the reservoir on the right hand and oozes out at the tunnel on the left hand of this figure. For simplicity, the effect of rainfall infiltration into the medium is not considered.

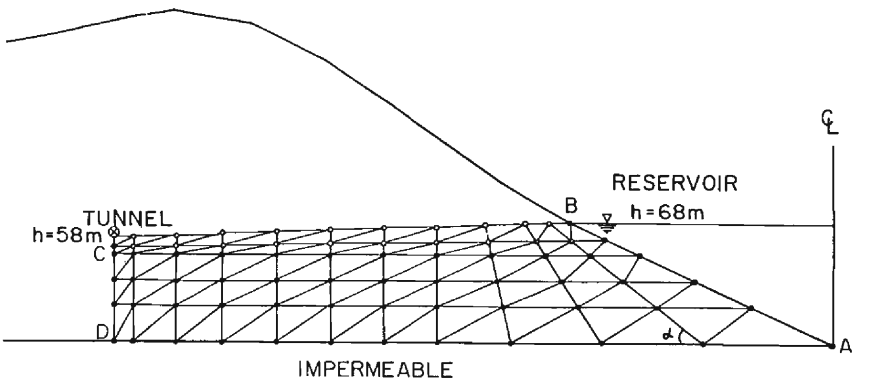

Fig. 12. Finite element model for shifting the free surface of groundwater (○: Movable node, and ●: fixed node).

In our first attempt to solve the seepage problems, the distribution of the free surface under the steady state condition is considered. The water level ($\bar{H}$) of the reservoir is kept to be at a constant elevation of 68.7 m which is about 10 m higher than the tunnel floor (H_0=58.0 m). Without losing generality, the atmospheric pressure is set to be zero. The flow domain shown as ABCD in **Fig. 12** is divided into 110 triangular elements with 72 nodes. These nodes are classified into two groups, i.e. movable nodes (○) and fixed ones (●). The distribution of hydraulic heads (h) in the domain ABCD has been determined using the finite element method under the following conditions; (1) hydraulic heads on faces AB and CD are set to be 68.7 m ($h=\bar{H}$) and 58.0 m ($h=H_0$), respectively, (2) the face DA is the horizontal boundary between permeable and impermeable media and there is no flow across the boundary, (3) an initial guess of the free surface of groundwater is given by the straight line connecting nodes B and C. In addition to these conditions, the hydraulic head (h) on the free surface must be equal to the elevation head (Z) of each corresponding node. Thus, the iteration was repeated until $|(h-Z)/Z| \leqq 0.0001$ by correcting positions of movable nodes along nodal lines. To facilitate such corrections, nodal lines are fixed by assigning angles α which they subtend with a bottom boundary (**Fig. 12**). As a result, the free surface BC forms a concave feature at the right hand near the reservoir and a convex feature at the left hand toward the tunnel. The maximum deviation of the free surface curve from the straight line is about 50 cm.

Next, we analyze the unsteady seepage problems where the free surface is continuously changing its position according to the draw-down of the water level of the reservoir. As an initial position of the free surface, we adopt the values obtained from the steady seepage analysis mentioned above. The distribution of hydraulic heads at time $t=t_0+n\Delta t$ is then determined by the 'step by step method' similar to that used by Komada and Kanazawa[20] for analyzing the unsteady seepage through fill dams. Boundary conditions are as follows: Hydraulic heads (h) of nodes on faces AB and BC are given by $h=\bar{H}(t)$ and $h=Z(y, z, t-\Delta t)$, respectively, where $\bar{H}(t)$ is the water level of the reservoir at time t, and $Z(y, z, t-\Delta t)$ is the elevation head on the free surface at time $t-\Delta t$. On faces CD and DA, boundary conditions are the same as those used in the analysis of the steady seepage problem.

The movement of free surface during the time interval of Δt is determined by considering the actual velocity (V) of the fluid particle lying on the free surface. The relationship between the actual velocity (V) and the seepage velocity (V_D), derived from Darcy's Law of Eq. 8, is expressed as follows (Yamagami[21]),

$$V = V_D/\beta \,, \tag{11}$$

where β is the effective porosity of the medium.

After a short time interval of Δt, coodinates of nodes on the free surface are modified by the amount of $V \times \Delta t$ along nodal lines and a new set of boundary conditions are derived. By repeating these procedures, the position of free surface and the distribution of hydraulic heads in the medium are determined in any arbitrary time.

Values of β obtained from field experiments for the various rocks of the world are distributed ovre a very wide range, that is to say, 43%~0.4%[22]. Since we have no experimental data about the effective porosity (β) of Palaeozoic formations of this region, we assume $\beta=5\%$ at present.

The field experiment for measuring the coefficient of permeability (k) in this region was made by Kadowaki and Daicho[23] at the Kisenyama rock fill dam which is located about 4 km above the Amagase dam (relative positions of these dams are shown in **Fig. 1(A)**). According to their results, k is within the range of 10^{-4}~10^{-7} m/sec for Palaeozoic formations consisting of shale, clay-slate, chert and sand-stone. In our calculations, we have adopted values of 10^{-4}, 10^{-5} and 10^{-6} m/sec.

Based on these values, we have calculated the distributions of hydraulic heads in the medium and the movements of free surface of groundwater. **Fig. 13(A)~(C)** show results from calculations for three cases of $k=10^{-4}$, 10^{-5} and 10^{-6} m/sec, respectively. The initial time ($t=0$) is 18 h on September 30 and Δt is set to be an hour. It can be seen from these figures that the movements of free surface are not so distinct except for the case of $k=10^{-4}$ m/sec, but equi-potential lines of hydraulic heads in the flow domain distinctly change with the lapse of time in any case.

Using these results, we next calculate the groundwater pressures in the medium. Then, we estimate strain field associated with the change of groundwater pressures

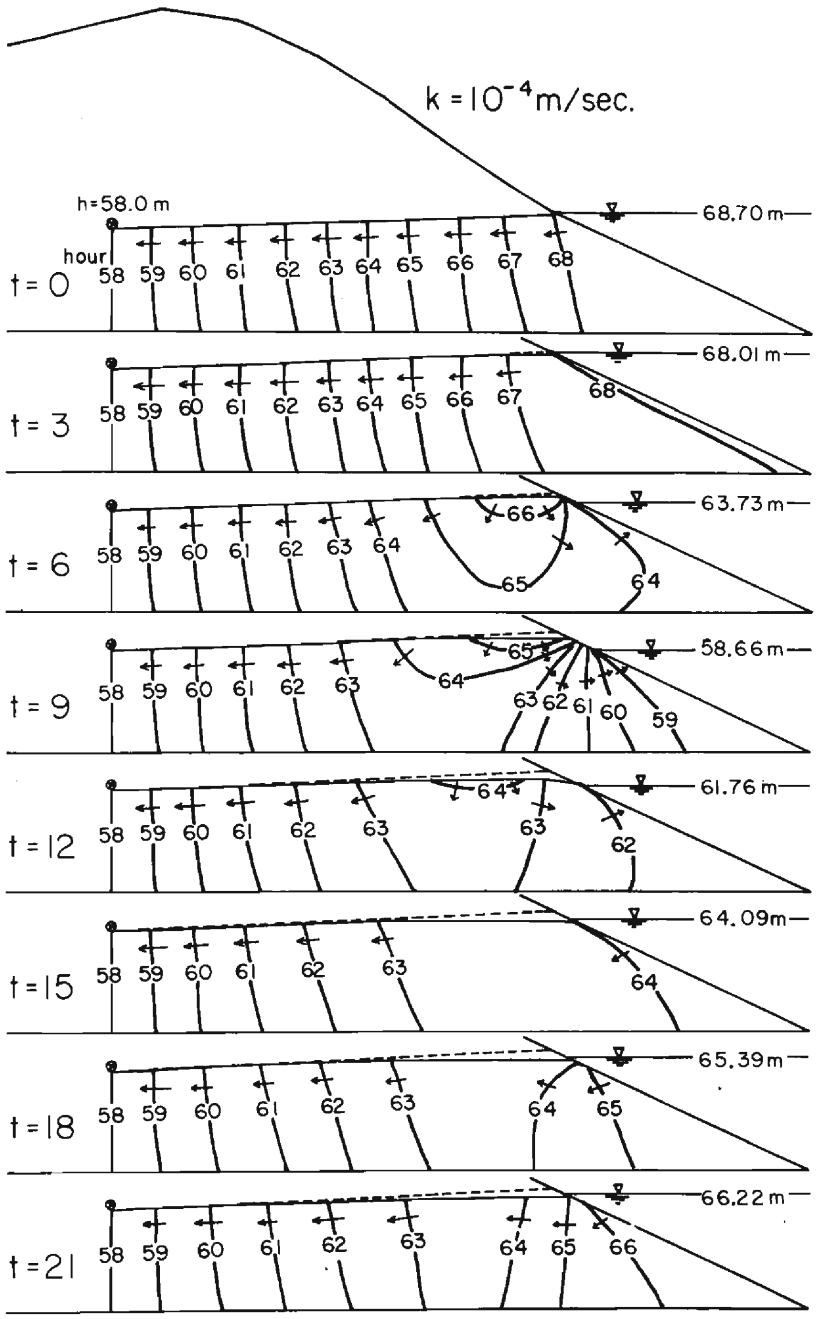

Fig. 13(A). Variations of equi-plotential inesl of ground water for $k=10^{-4}$ m/sec (arrow shows the stream direction).

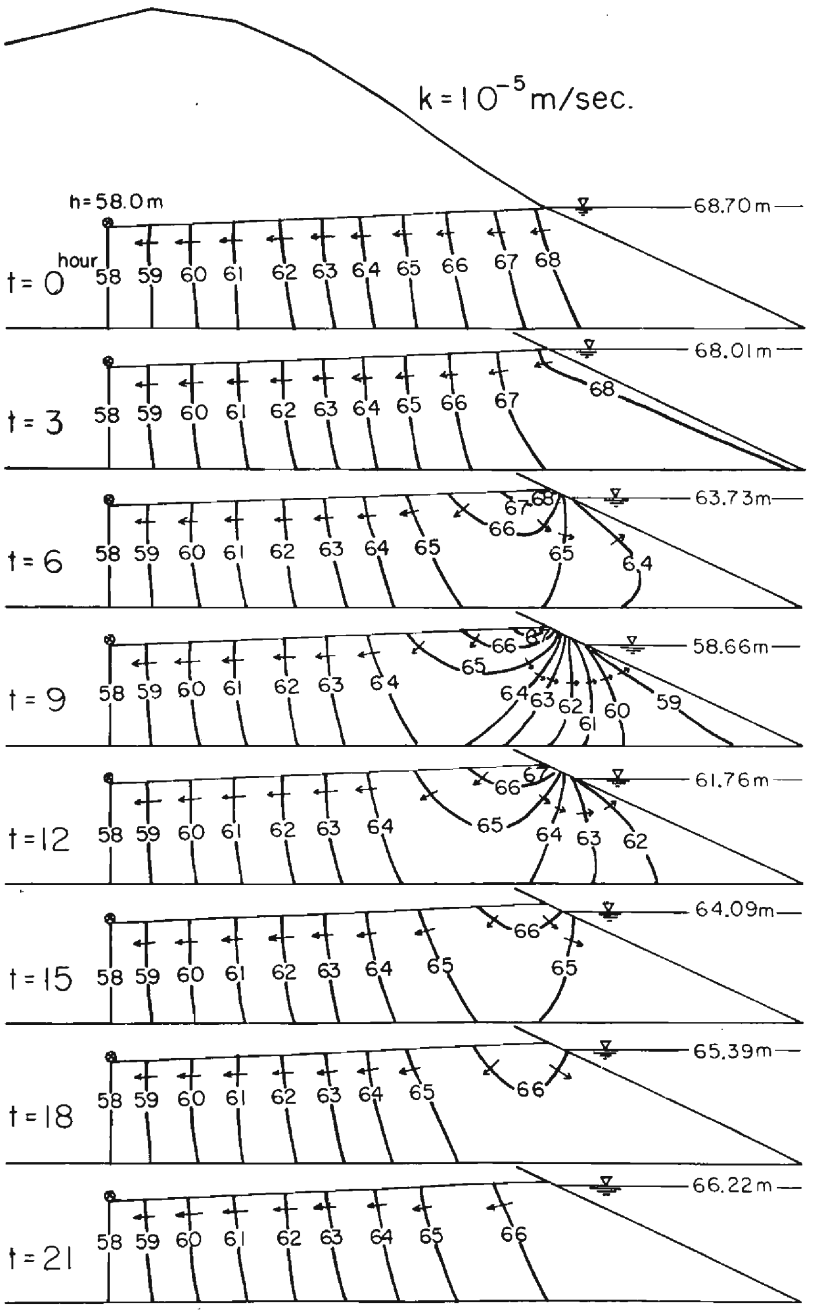

Fig. 13(B). Variations of equi-potential lines of groundwater for $k=10^{-5}$ m/sec (arrow shows the stream direction).

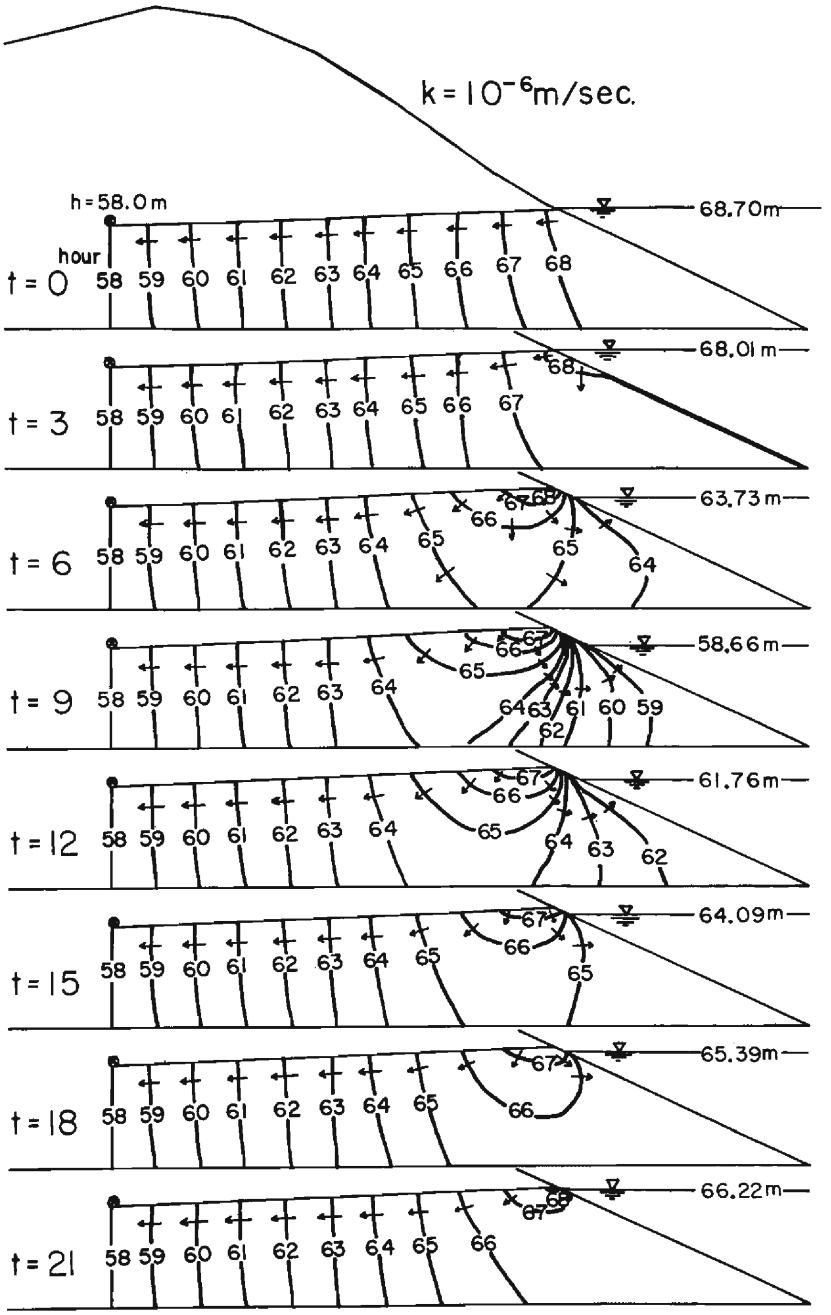

Fig. 13(C). Variations of equi-potential lines of groundwater for $k=10^{-6}$ m/sec (arrow shows the stream direction).

due to the rapid draw-down of the water level of the reservoir.

5.2.2 Strain Fields Associated with Changes of Groundwater Pressures in Porous Media

Effects of groundwater pressures on strains in porous media can be considered as primarily due to a body force proportional to the gradient of hydraulic heads and a secondary hydrostatic compression due to the compressibility of the solid component (Zienkiewicz[24]). In many materials such as concrete or rock, the strains due to the secondary effect are practically negligible and only the primary effect is of importance.

We now consider these body forces in a triangular element with nodes i, j and m. A body force R_y in the horizontal direction (y) is expressed as follows,

$$R_y = (T/2) \times \{H_i(z_m - z_j) + H_j(z_i - z_m) + H_m(z_j - z_i)\} , \tag{12}$$

where T is the thickness of the element, $H_{i\sim m}$ is the hydraulic head and $z_{i\sim m}$ is the coordinate in the vertical direction of the corresponding node, respectively. The vertical component of body force R_z is evaluated by a similar expression by changing z to y symbols. If groundwater pressures in pores are considered as body forces in the porous medium, external water forces are automatically included in calculations and the effective normal stress is considered to be zero (Zienkiewicz and Cheung[25]).

The assignment of the resultant of body forces to nodes can be made by using

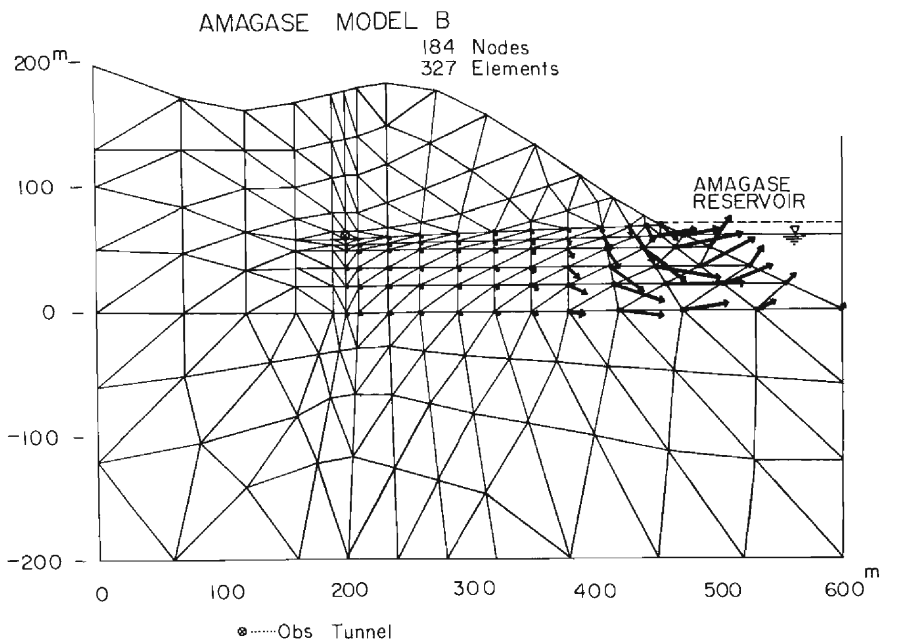

Fig. 14. Finite element model expressing the region of about 1000×400 m with 327 triangular elements and nodal forces equivalent to change of groundwater pressure.

the same procedure as that dealing with the gravity forces in finite element calculations. Nodal forces equivalent to distributed body forces in the element are defined by allocating in three equal parts ($R_y/3$ and $R_z/3$) to each node. As an example of equivalent nodal forces, **Fig. 14** shows vector expressions of these forces associated with the change of groundwater pressures from the steady state ($t=0$ hour) to the state of the maximum draw-down of the water level ($t=9$ hour), where k is set to be 10^{-6} m/sec.

Residual strain fields due to these nodal forces were calculated by the finite element techniques for the model expressing the region of about 1000 m $\times$ 400 m with 327 triangular elements (**Fig. 14**). Results of calculations are shown in **Fig. 15(A)**$\sim$**(C)** for three cases of $k=10^{-4}$, 10^{-5} and 10^{-6} m/sec, respectively. At the position of the observation tunnel ($\otimes$), the linear strain of y direction (e_{yy}) is within the range of $1.8\sim2.0\times10^{-7}$ and that of z direction (e_{zz}) is about -0.9×10^{-7} in any case of **Fig. 15 (A)**$\sim$**(C)**. These values are not so much affected by the difference of k, and are roughly consistent with observed ones.

Subsequently, we estimate the strain field around the observation tunnel taking the cavity effect into consideration.

5.2.3. Expected Strain Field Including the Cavity Effect

Postulating the plane strain condition, we have calculated the strain field induced by the variation of groundwater pressures during the time interval from $t=0$ (hour) to $t=9$ (hour). Strains over four elements adjacent to the observation tunnel are averaged. In the absence of cavity, these values are obtained as follows for the case of $k=10^{-6}$ m/sec,

$$\begin{aligned} e_{yy} &= 1.95\times10^{-7} \\ e_{zz} &= -0.97\times10^{-7} \\ e_{yz} &= -0.12\times10^{-7}, \end{aligned}$$

and similarly principal stresses in the y-z plane are,

$$\begin{aligned} \sigma_{\max} &= 9.04\times10^{3}\ \mathrm{N/m^2} \\ \sigma_{\min} &= -1.26\times10^{3}\ \mathrm{N/m^2} \\ \theta &= 1.23^\circ, \end{aligned}$$

where θ is the inclination of the axis of $\sigma_{\max}$ with respect to y measured in the $y-z$ plane.

We now consider the cavity effect on strains using the same procedure as mentioned in section 4. Without losing generality, it may be permitted to set $\sigma_y=\sigma_{\max}$ and $\sigma_z=\sigma_{\min}$ because θ is negligibly small. Therefore, nodal forces equivalent to $\sigma_y(=\sigma_{\max})$ are applied on face BC of the two-dimensional finite element model which is shown on the left hand of **Fig. 9.** Similarly, nodal forces equivalent to

$\sigma_z(=\sigma_{min})$ are applied on faces EB and FC of the model. Along the line EF, nodal displacements in the y direction are fixed to be zero. As a result, strains including the cavity effect are obtained as follows at the place where the instruments are installed,

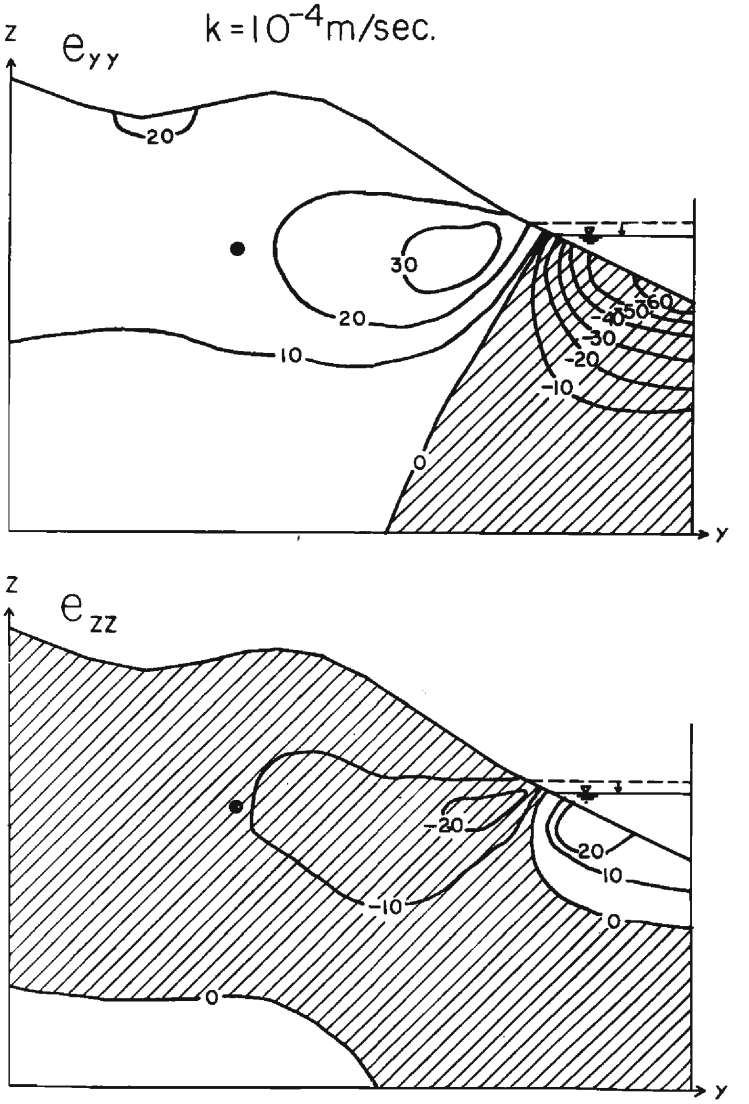

Fig. 15(A). Distributions of strains associated with variations of groundwater pressure in a porous medium for the case of $k=10^{-4}$ m/sec ($\times 10^{-8}$).

$$e^c_{yy} = \quad 4.75\times10^{-7}$$
$$e^c_{zz} = -2.56\times10^{-7}.$$

These values are 2.4~2.6 times larger than e_{yy} and e_{zz} which have been calculated previously in the absence of the cavity. Differences are reasonable as cavity effects. Then, we compare these values with observational results.

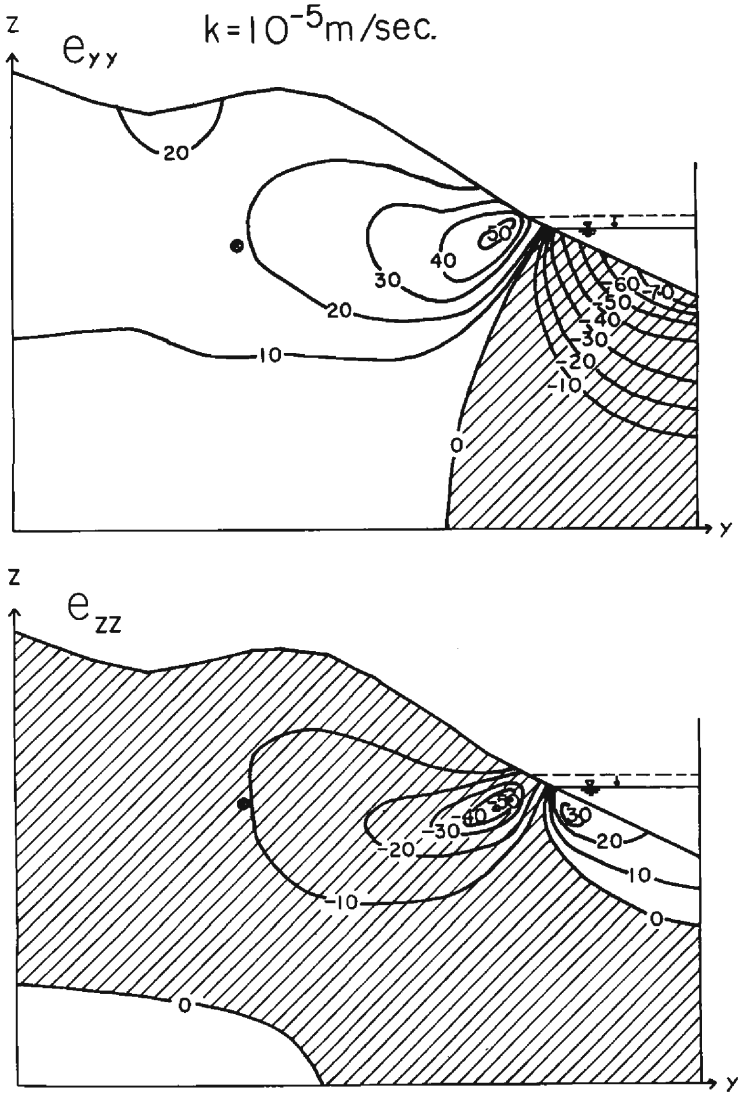

Fig. 15(B). Distributions of strains associated with variations of groundwater pressure in a porous medium for the case of $k=10^{-5}$ m/sec ($\times10^{-8}$).

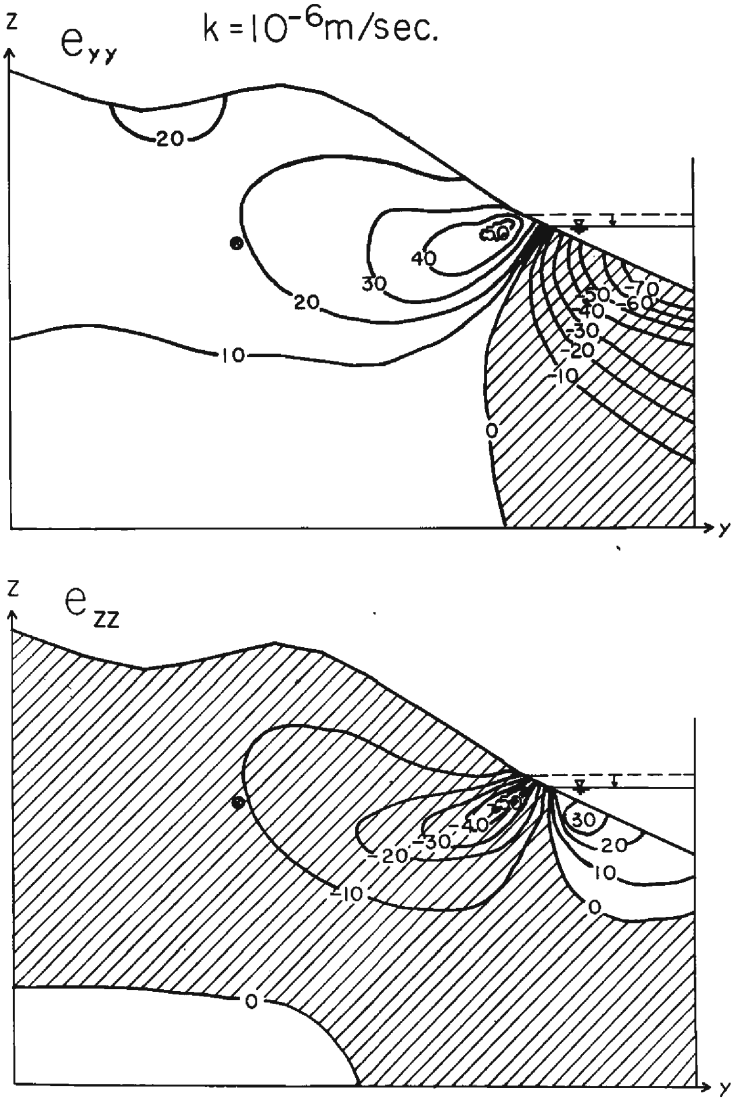

Fig. 15(C). Distributions of strains associated with variations of ground-water pressure in a porous medium for the case of $k=10^{-6}$ m/sec ($\times 10^{-8}$).

6. Comparison between Observed and Theoretically Expected Strains

Rearranging the whole aspect described in previous sections, we show in **Fig. 16** the variations of the barometric pressure, the water level of the reservoir, observed ground-strains in y and z directions, and theoretically expected strains including cavity effects in corresponding directions for the period from September 30 to October 01. It is obvious from this figure that the observed ground-strains are not

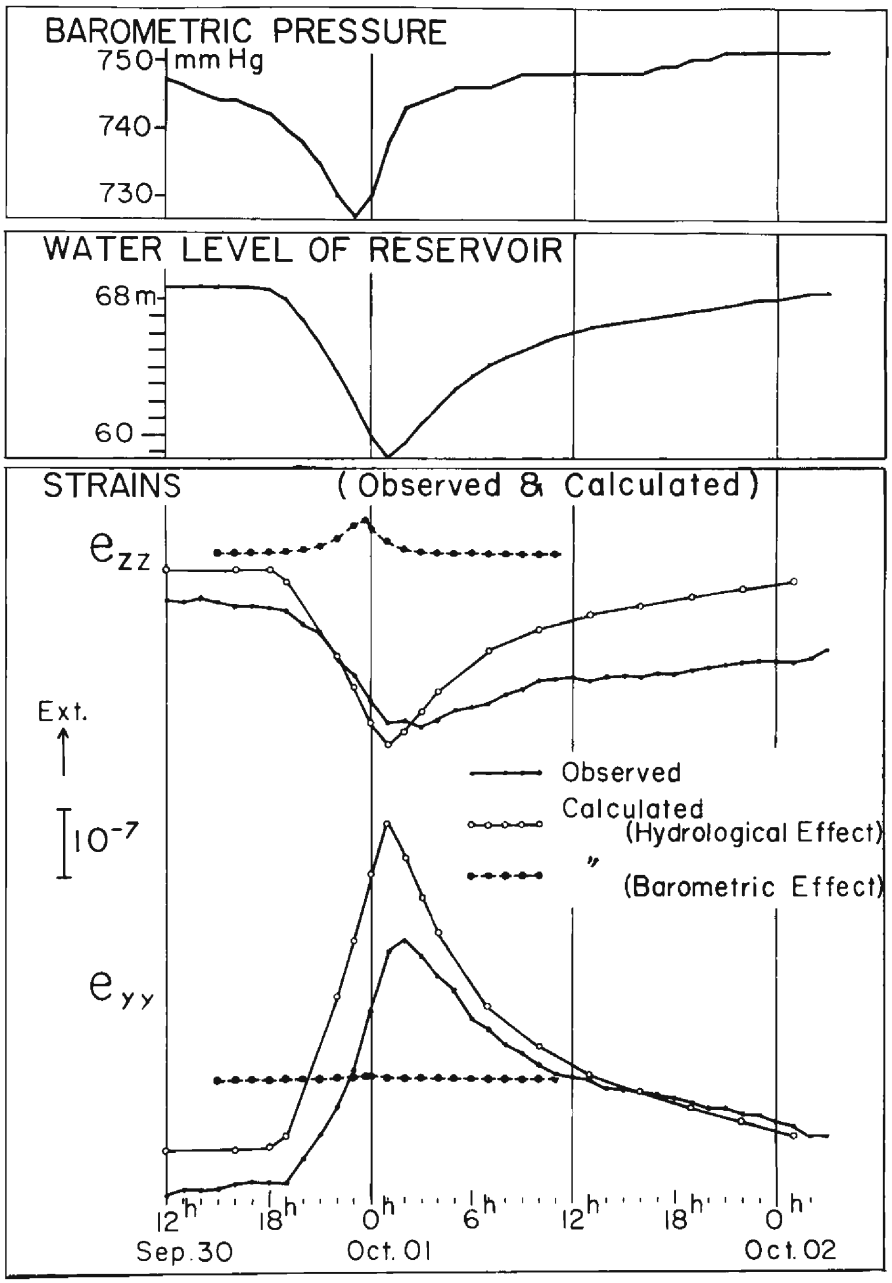

Fig. 16. Hourly variations of barometric pressure (upper), water level of reservoir (middle), and observed and theoretically expected strains (lower).

consistent with the theoretical curves obtained for the atmospheric loading effect due to the passage of the typhoon but consistent with the theoretical curves obtained for the hydrological effect due to the rapid draw-down of the reservoir.

As a result, observed strains of the order of 10^{-7} can be successfully explained by the hydrological model considering the effect of groundwater pressures under the rapid draw-down of the water level of the reservoir. In this case, better fit to observational results will be possible by changing the value of effective porosity (β).

7. Conclusions

Using continuous records obtained from four extensometers with laser interferometer systems at the Amagase Observatory, meteorological and hydrological perturbations on ground-strain measurements have been investigated and the following results are obtained.

(1) Seasonal variations of ground-strains of the order of 10^{-6} are observed with components installed in the plane normal to the axis of the tunnel (L–2 and EL–V). On the other hand, seasonal variations observed with components along the tunnel (L–1 and EL–1) are smaller than the order of 10^{-7} in a strain amplitude. These variations cannot be considered to be caused by the thermal effect due to the seasonal variation of air temperature. The effect of rainfall on ground-strains is not so distinct except for the period of a heavy rainfall of 216 mm from the end of June to early July, 1979. According to this heavy rainfall, the L–2 component contracted to the amount of 0.9×10^{-6} and the EL–V component extended to the amount of 0.5×10^{-6}. Contributions from the level changes of the nearby reservoir do not exceed the order of 10^{-7} in a strain amplitude. As a whole, seasonal variations of the order of 10^{-6} in L–2 and EL–V components cannot be explained by the independent effects as mentioned above.

(2) After removing seasonal variations from original data, there remain transient variations with a strain amplitude of the order of 10^{-7} in L–2 and EL–V components. Transient variations of this sort are not found in L–1 and EL–1 components. These variations cannot be explained by the elastic strains caused by negative surface-loads due to the passage of a typhoon or due to the rapid draw-down of the water level of the reservoir. Strains expected for these elastic models are at the most the order of 10^{-8}. In order to explain observational results with a strain amplitude of the order of 10^{-7}, we considered the seepage of groundwater in a porous medium and analyzed stress-strain relations around the tunnel by taking the variation of groundwater pressure into consideration. As a result, theoretically expected strains for this permeable model under the rapid draw-down of the water level of the reservoir are well consistent with observed values.

(3) Based on this aspect, we reconsider the seasonal variations of ground-strains. There exist some common features between the seasonal variations and the transient variations caused by the rapid draw-up or draw-down of the water level of the re-

servoir; (I) ground-strains observed with the horizontal components along the tunnel are negligibly small, (II) ground-strains observed with the horizontal and vertical components in the plane normal to the axis of the tunnel have large amplitudes with opposite sign, i.e. when one is in extension, the other is in contraction. And the amplitude ratio between them is about 2:1. These facts suggest that both cases can be explained by the same mechanism. Therefore, we consider the seasonal variations of ground-strains are also associated with the hydrological effect due to seasonal variations of groundwater pressure in the porous medium around the tunnel. Seasonal variations of groundwater pressure may be complicatedly related to the amount of rainfall, variations of the water level and water discharge of the reservoir.

(4) In Paper II, we have previously compared the observed and theoretically expected tidal strains of M_2 and O_1 constituents. Taking the cavity and topographic effects into consideration, there remain discrepancies in the direction across the tunnel, i.e. observed values are 33~52% larger than the theoretically expected ones. On the other hand, observed values in the direction along the tunnel are consistent with the expected ones within an error inherent in numerical calculations. These results may also be explained as the hydrological effect due to the daily variation of groundwater pressure around the tunnel.

(5) It must be noted that the effect of rainfall on ground-strains have something in common at several observatories where ground-strain measurements in the plane normal to the axis of the tunnel were or have been carried on (Ide (Takada[4]), Iwakura (Takada et al.[26]) and Miyasaki (Takada et al.[27])). Drawing a common feature from these observational results, the amount of discharge of groundwater in the tunnel suddenly increases after a rainfall and accordingly the horizontal strain across the tunnel shows the contraction and the vertical strain shows the extension. At that time, the horizontal strain along the tunnel is relatively small. This feature of strain accumulation around the tunnel is consistent with that obtained at the Amagase Observatory for the period of the heavy rainfall or the rapid draw-up of the water level of the reservoir as shown schematically in **Fig. 4.** Therefore, it can be considered as a first approximation that the effect of rainfall on ground-strain measurements in a tunnel near the earth's surface is explained by the same mechanism of hydrological perturbations taking the seepage problem of groundwater into consideration.

Acknowledgements

The author wishes to express his sincere thanks to Prof. Michio Takada, Dr. Torao Tanaka and Dr. Tamotsu Furuzawa for their encouragement and helpful suggestions during the course of this work.

The author is much indebted to Prof. Kazuo Ashida for getting hydrological data of the Amagase Reservoir.

Thanks are also due to Mr. Toshio Kobayashi for his cooperation in improvement of laser extensometers and to Mr. Masaru Yamada and Mr. Akio Hirono for their help in maintenance of instruments.

The computations involved were made at the Information Data Processing Center for Disaster Prevention Research, of the Disaster Prevention Research Institute, Kyoto University.

References

1) Takemoto, S.: Laser interferometer systems for precise measurements of ground-strains, Bull. Disas. Prev. Rec. Inst., Kyoto Univ., Vol. 29, Part 2, No. 262, 1979, pp. 65–81.
2) Takemoto, S. and T. Kobayashi: On the laser extensometer with a simple laser source, Annuals Disas. Prev. Res. Inst., Kyoto Univ., No. 25 B–1, 1982, pp. 31–39 (in Japanese).
3) Takemoto, S.: Effects of local inhomogeneities on tidal strain measurements, Bull. Disas. Prev. Res. Inst., Kyoto Univ., Vol. 31, Part 4, No. 284, 1981, pp. 211–237.
4) Takada, M.: On the observation of the crustal deformation and meteorological effects on it at Ide observatory, Bull. Disas. Prev. Res. Inst., Kyoto Univ., Vol. 8, No. 23, 1958, pp. 1–12.
5) Takemoto, S.: The observation of crustal deformations at Iwakura, Kyoto, (I), Annuals Disas. Prev. Res. Inst., Kyoto Univ., No. 10A, 1967, pp. 157–164 (in Japanese).
6) Takada, M., T. Furuzawa, S. Takemoto and M. Yamada: The observation of crustal deformations at Iwakura, Kyoto, (IV), Annuals Disas. Prev. Res. Inst., Kyoto Univ., No. 17B, 1974, pp. 57–62 (in Japanese).
7) Tanaka, T.: Study on meteorological and tidal influences upon ground deformations, Special Contributions Geophys. Inst., Kyoto Univ., No. 9, 1969, pp. 29–90.
8) Takemoto, S.: Strain changes caused by the change of the water level of the reservoir, Jour. Geodetic Soc. Japan, Vol. 28, No. 1, 1982, pp. 41–50 (in Japanese).
9) Takada, M., K. Onoue, T. Kobayashi and M. Yamada: On the observation of the crustal deformation at Amagase observatory (Preliminary Report), Annuals Disas. Prev. Res. Inst., Kyoto Univ., No. 11A, 1968, pp. 213–220 (in Japanese).
10) Takada, M., T. Furuzawa, S. Takemoto and M. Yamada: Observation of crustal deformation at Amagase observatory, Jour. Geodetic Soc. Japan, Vol. 27, No. 4, 1981, pp. 293–296.
11) Nakajima, C., Y. Mitsuta, Y. Gocho, M. Tanaka, T. Fujii and N. Monji: On typhoon 7916, Annuals Disas. Prev. Res. Inst., Kyoto Univ., No. 23B–2, 1980, pp. 87–111 (in Japanese).
12) Trubitsyn, A.P. and A.B. Makalkin: Deformations of the earth's crust under the action of atmospheric cyclones, Izv. Acad. Sc. USSR, Earth Phys., No. 5, 1976, pp. 94–96 (in Russian).
13) Panek, L.A.: Calculation of the average ground-stress components from measurements of the diametral deformation of a drill hole, Testing Techniques for Rock Mechanics, ASTM STP 402, Am. Soc. Testing Mats,. 1966, pp. 106–132.
14) Zienkiewicz, O., P. Mayer and Y.K. Cheung: Solution of anisotropic seepage by finite elements, Proc. ASCE, Vol. 92, No. EM 1, 1966, pp. 111–120.
15) Taylor, R.L. and C.B. Brown: Darcy flow solutions with a free surface, Proc. ASCE, Vol. 93, No. HY 2,1967, pp. 25–33.
16) Finn, W.D.L.: Finite-element analysis of seepage through dams, Proc. ASCE, Vol. 93, No. SM 6, 1967, pp. 41–48.
17) Kawamoto, T., H. Komada and T. Miyaguti: Analyses of seepage through dams and in foundation by finite element method, Soil Mechanics and Foundation Engineering, Vol. 18, No. 12, 1970, pp. 19–26 (in Japanese).
18) France, P.W., C.J. Parekh, J.C. Peters and C. Taylor: Numerical analysis of free surface seepage problems, Proc. ASCE, Vol. 97, No. IR1, 1971, pp. 165–179.
19) Desai, C.S.: Seepage analysis of earth banks under drawdown, Proc. ASCE, Vol. 98, No. SM 11, 1972, pp. 1143–1162.

20) Komada, H. and K. Kanazawa: Analysis of unsteady seepage flow and stability of fill dams under rapid drawdown of the water surface level of reservoirs, Proc. Japan Soc. Civil Engineers, No. 240, 1975, pp. 51–62 (in Japanese).
21) Yamagami, T.: A study on the finite element solution of transient seepage under drawdown, Proc. Japan Soc. Civil Engineers, No. 263, 1977, pp. 85–95 (in Japanese).
22) Chigaku-jiten (Lexicon of Physical Geography), Heibon-sha Co., Ltd., Tokyo, 1970 (in Japanese).
23) Kadowaki, K. and A. Daicho: On the spatial examination of the design of the Kisenyama rock-fill dam, Hydro Electric Power, No. 98, 1969, pp. 8–27 (in Japanese).
24) Zienkiewicz, O.C.: Stress analysis of hydraulic structures including pore pressure effects, Water Power, Vol. 15, 1963, pp. 104–108.
25) Zienkiewicz, O.C. and Y.K. Cheung: Stresses in buttress dams, Water Power, Vol. 17, 1965, pp. 69–75.
26) Takada, M., T. Furuzawa, S. Takemoto and M. Yamada: Effects of amounts of rainfall and discharged water upon the ground-strain at the Iwakura observatory, Annuals Disas. Prev. Res. Inst., Kyoto Univ., No. 24B–1, 1981, pp. 71–76 (in Japanese).
27) Takada, M., T. Furuzawa, S. Takemoto, K. Onoue, M. Teraishi and Y. Sonoda: Observations of the crustal movement at the Miyazaki crustal movement observatory (1), Annuals Disas. Prev. Res. Inst., Kyoto Univ., No. 22B–1, 1979, pp. 61–77 (in Japanese).